

## Supporting Information

# Regulating electronic structure of CoMoO<sub>4</sub> by La-Doping for Efficient and Durable Electrochemical Water Splitting Reactions

*Bharathi Arumugam,<sup>a</sup> Erakulan E. Siddharthan,<sup>b</sup> Pandian Mannu,<sup>c</sup> Ranjit Thapa,<sup>b,d</sup> Chung-Li Dong,<sup>c</sup> Arokia Anto Jeffery,<sup>\*e</sup> Seong-cheol Kim<sup>\*a</sup>*

<sup>a</sup>Department of Chemical Engineering, Yeungnam University, Gyeongsan, 38541, Korea

<sup>b</sup>Department of Physics, SRM University–AP, Amaravati, Andhra Pradesh, 522 240, India

<sup>c</sup>Department of Physics, Tamkang University, New Taipei City 25137, Taiwan

<sup>d</sup>Center for Computational and Integrative Sciences, SRM University–AP, Amaravati, Andhra Pradesh, 522 240, India

<sup>e</sup>Department of Bioengineering, Saveetha School of Engineering, Saveetha Institute of Medical and Technical Sciences (SIMATS), Chennai-602105, India

### **Computational details:**

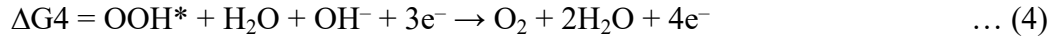
All the spin-polarized density functional theory calculations are performed in the Vienna Ab initio Simulation Package (VASP)<sup>1</sup>. The projected Augmented Wave (PAW) method is used to describe the potentials of the atoms with Generalized Gradient Approximation (GGA) is considered for exchange and correlation effects at the Perdew-Burke-Ernzerhof (PBE) level<sup>2,3</sup>. Plane-wave cut-off energy of 450 eV is used for the calculations. A 3x3x1 K-point grid is used for the Brillouin zone sampling for adsorption studies and 9x9x1 for the density of states with the Monkhorst Pack scheme. Structural optimizations were carried out until the total energy converged less than  $10^{-5}$  eV per atom and the maximum force converged less than 0.01 eV/Å. Grimme's DFT-D3 with Becke-Johnson damping function method was taken for Van der Waals dispersion correction<sup>4,5</sup>. For the structure model, bulk CoMoO<sub>4</sub> was taken and cleaved into 003 plane with lattice parameters a, b = 13.04 Å, and c = 22.45 Å. The supercell model has three layers, of which the bottom two layers of metal and oxygen were fixed. The model contains 24 Co atoms, 24 Mo atoms, and 96 oxygen atoms for the pure CoMoO<sub>4</sub>. A vacuum of ~15 Å was taken in the z-direction to avoid periodic interaction. The CoMoO<sub>4</sub> unit cell was first optimized to determine its equilibrium geometry. Lanthanum was substituted at the Co sites to generate the doped structures. The doping concentration was set to 5% by replacing one Co in a 3x3x1 supercell of CoMoO<sub>4</sub>. The Fermi level was set to zero, and the shifts in the density of states near the Fermi level were carefully examined to understand the effects of doping on the material's electronic properties. To evaluate the catalytic activity for the hydrogen evolution reaction (HER) and oxygen evolution reaction (OER), the adsorption energies of key intermediates (H\*, OH\*, OOH\*) on the surface of CoMoO<sub>4</sub> and 5% La<sub>x</sub>CoMoO<sub>4</sub> were calculated. The adsorption sites were identified based on the surface geometry, and the most stable adsorption configurations were determined through geometry optimizations.

The adsorption energy ( $E_{\text{ads}}$ ) of an intermediate species was calculated using the formula:

$$E_{\text{ads}} = E_{\text{system+adsorbate}} - E_{\text{system}} - E_{\text{adsorbate}}$$

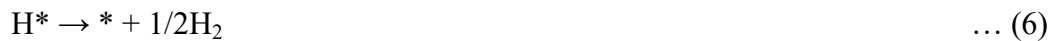
where  $E_{\text{system+adsorbate}}$  is the total energy of the CoMoO<sub>4</sub> system with the adsorbed species,  $E_{\text{system}}$  is the energy of the clean CoMoO<sub>4</sub> surface, and  $E_{\text{adsorbate}}$  is the energy of the isolated adsorbate species.

For the OER activity, free energy is calculated using the following equations,



Here \* represents the active site on the surface and the equations are given for the alkaline medium.

For HER, the activity is calculated through the following free energy equations,



The reaction pathways for HER and OER on the CoMoO<sub>4</sub> and 5% La<sub>–</sub>CoMoO<sub>4</sub> surfaces were investigated by calculating the free energy changes for each reaction step. The overpotential ( $\eta$ ) for HER was determined by evaluating the free energy change of the hydrogen adsorption step, while for OER, the overpotentials were derived from the potential-determining step involving the formation of OOH\*.

The overall overpotential was calculated as:

$$\eta_{OER} = \max (\Delta G_{\text{step } 1}, \Delta G_{\text{step } 2}, \Delta G_{\text{step } 3}, \Delta G_{\text{step } 4}) - 1.24 \text{ V}$$

$$\eta_{HER} = \Delta G_{H^*} - 0 \text{ eV}$$

where  $\Delta G$  represents the Gibbs free energy change for each reaction step.

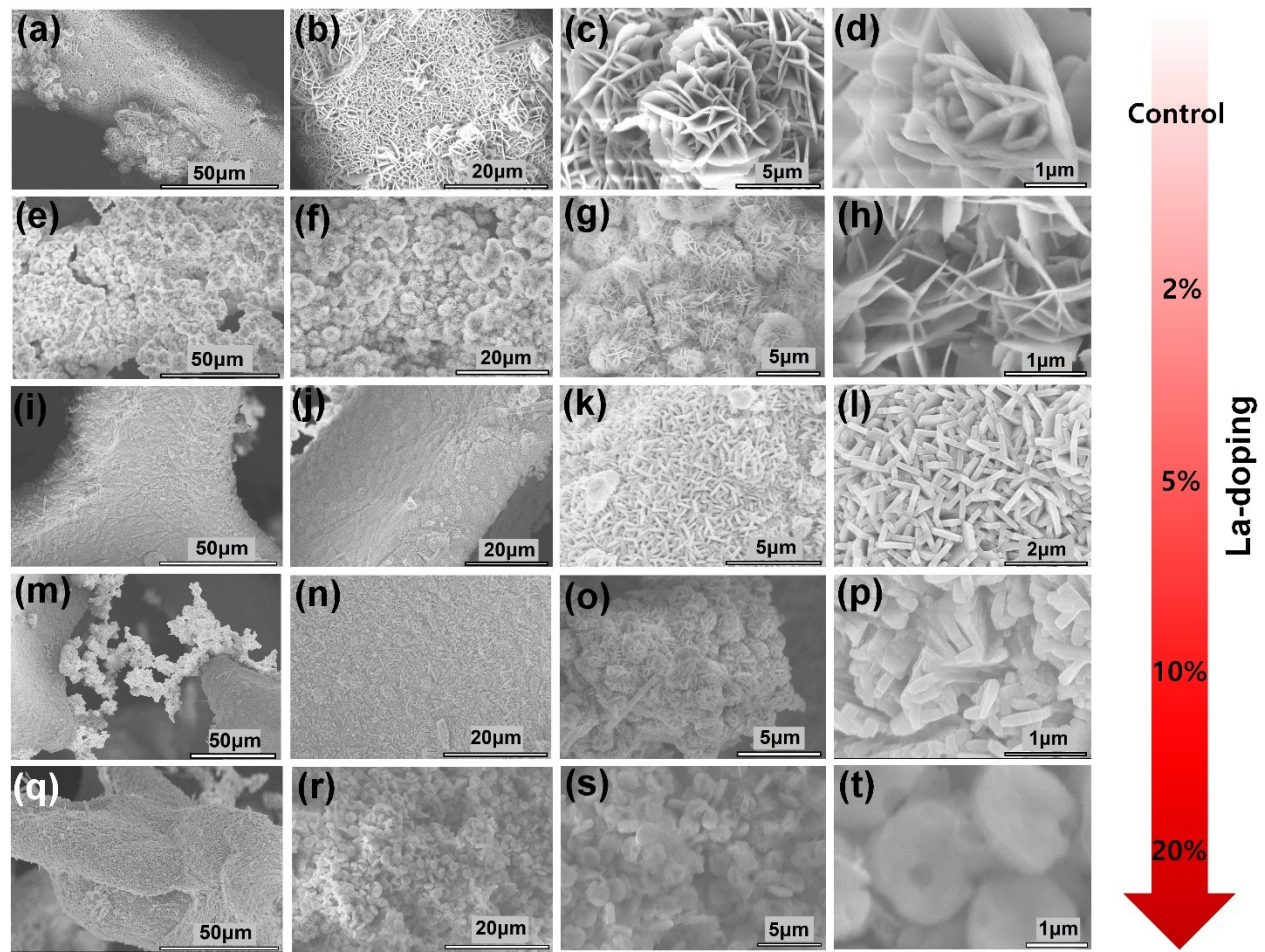


**Figure S1.** FESEM image of various La-doped CoMoO<sub>4</sub> and control catalysts, (a-d) Bare CoMoO<sub>4</sub>, (e-h) 2% La<sub>x</sub>CoMoO<sub>4</sub>, (i-l) 5% La<sub>x</sub>CoMoO<sub>4</sub>, (m-p) 10% La<sub>x</sub>CoMoO<sub>4</sub>, (q-t) 20% La<sub>x</sub>CoMoO<sub>4</sub>.

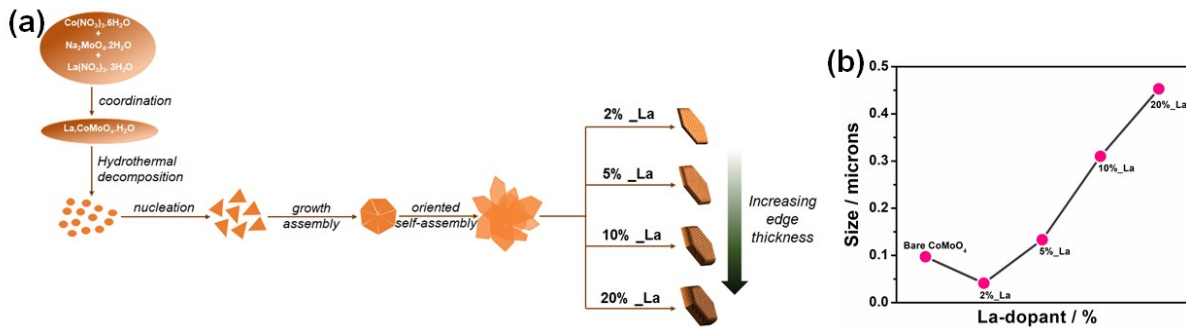


**Figure S2.** (a) Schematic representation depicting oriented self-assembly mechanism, (b) edge size vs. La-dopant concentration plot.

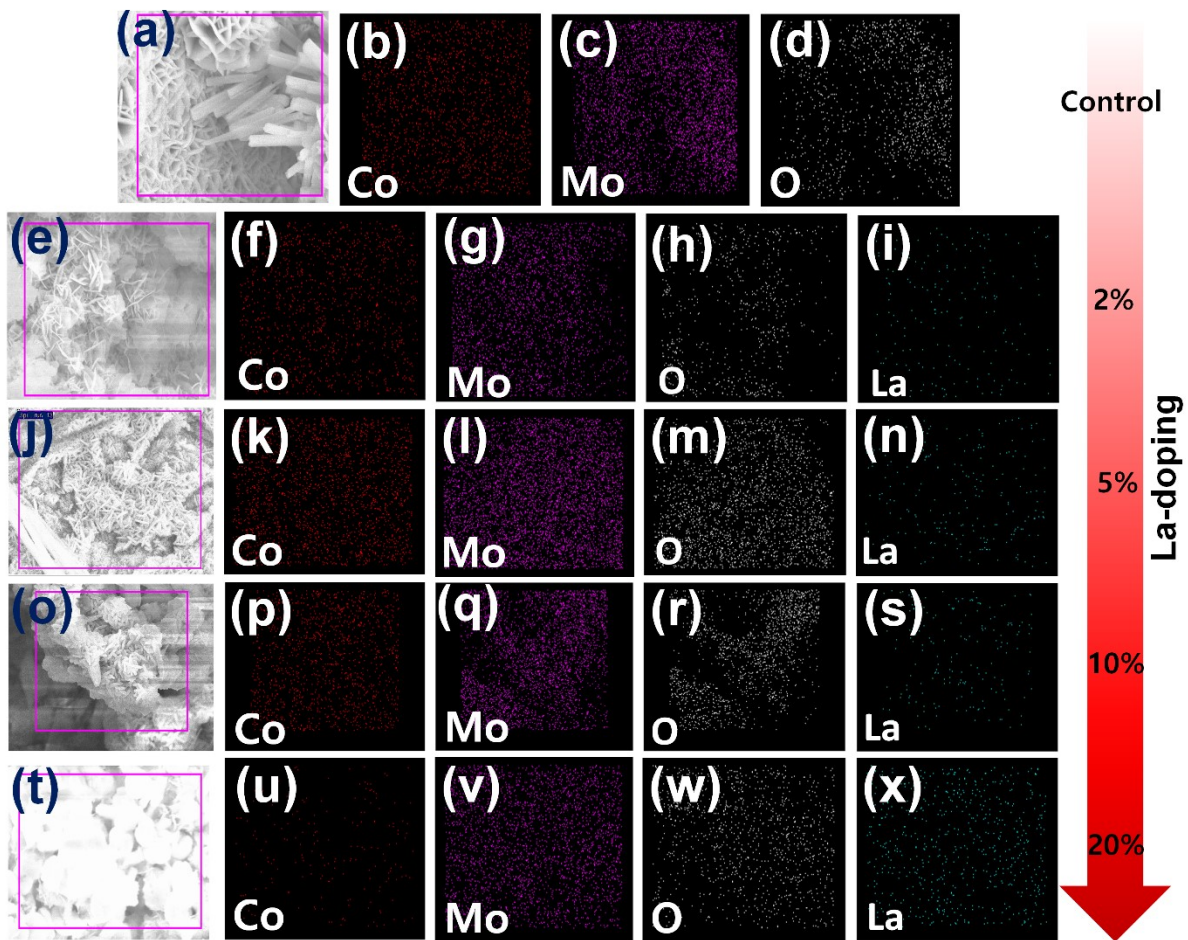


**Figure S3.** FESEM and corresponding energy dispersive X-ray (EDS) mapping analysis of a) Bare CoMoO<sub>4</sub>, b) 2% La\_CoMoO<sub>4</sub>, c) 5% La\_CoMoO<sub>4</sub>, d) 10% La\_CoMoO<sub>4</sub>, e) 20% La\_CoMoO<sub>4</sub>.

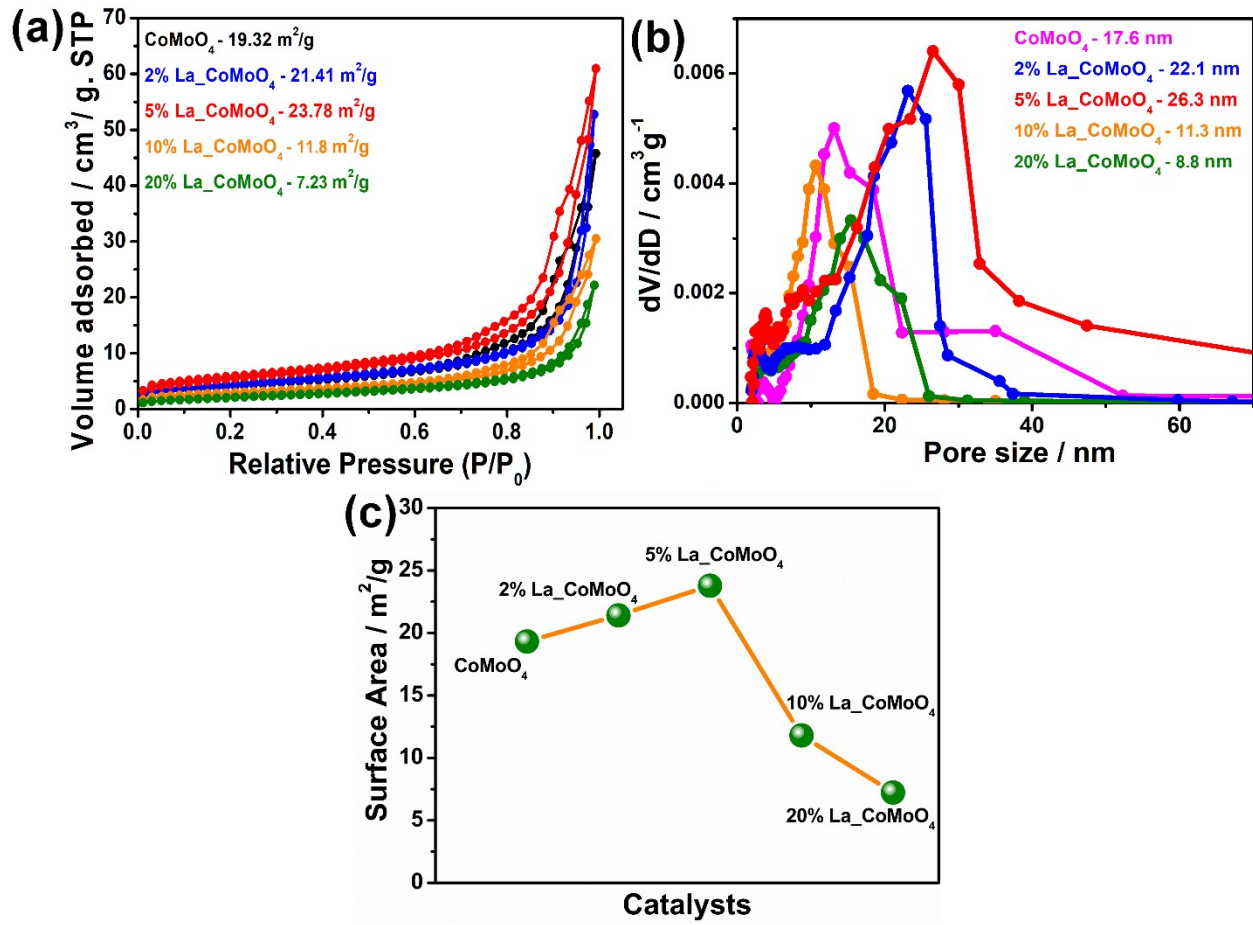


**Figure S4.** (a) BET isotherms and (b) BJH pore size distribution plots of bare CoMoO<sub>4</sub> and different percentages of La-doped CoMoO<sub>4</sub> catalysts, (c) surface area comparison plot of different catalysts obtained from BET isotherms.

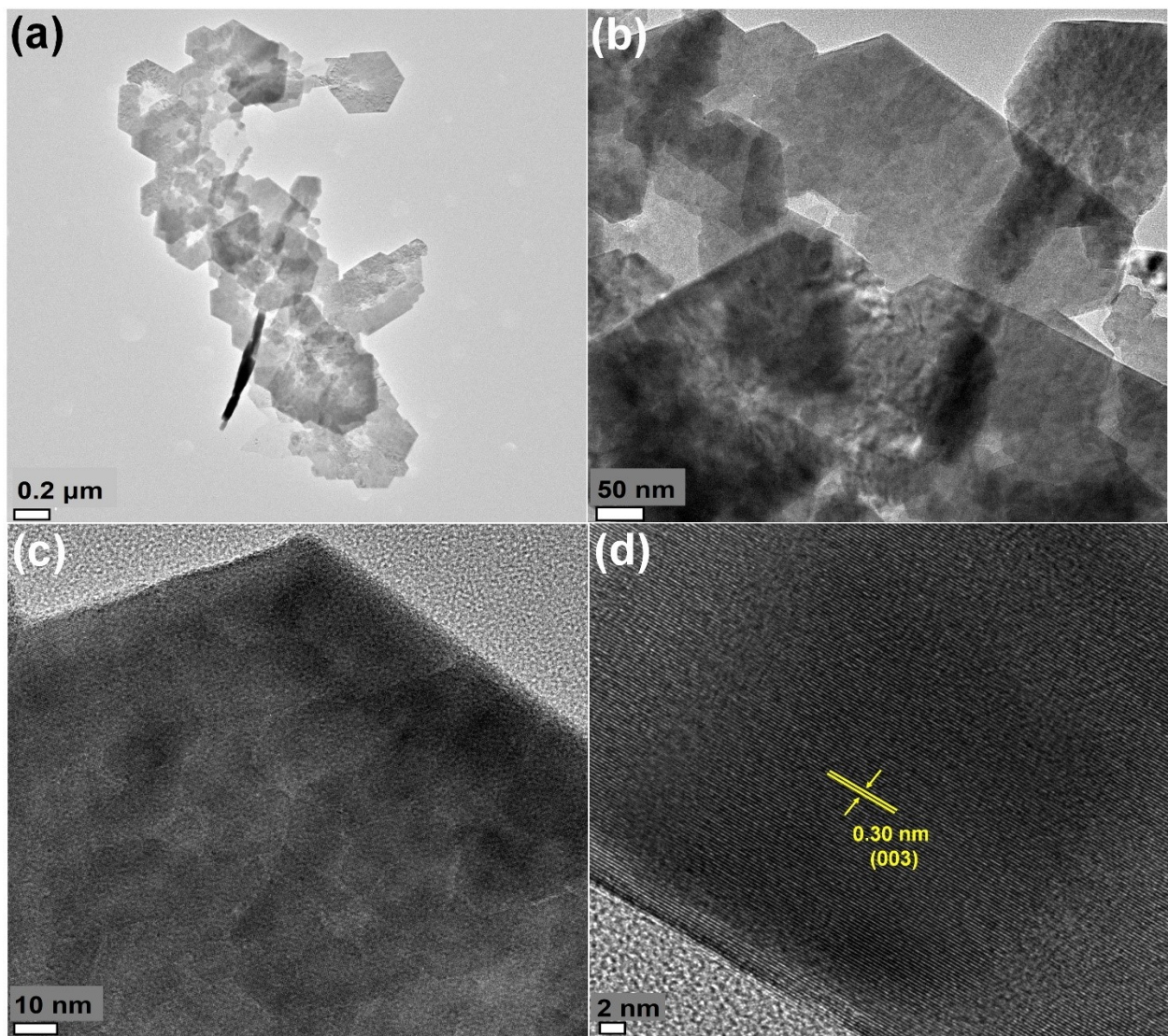


**Figure S5.** (a-d) TEM and HRTEM images of bare  $\text{CoMoO}_4$ .

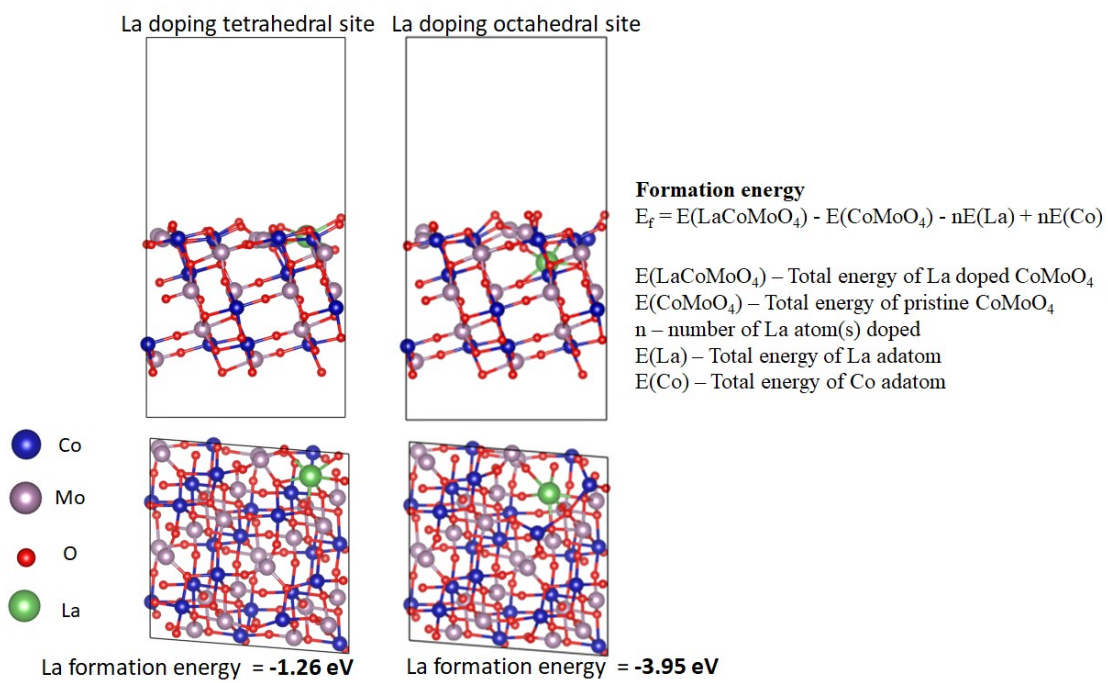


**Figure S6.** La-doped  $\text{CoMoO}_4$  structural models and the formation energy for La-dopant at tetrahedral and octahedral sites.

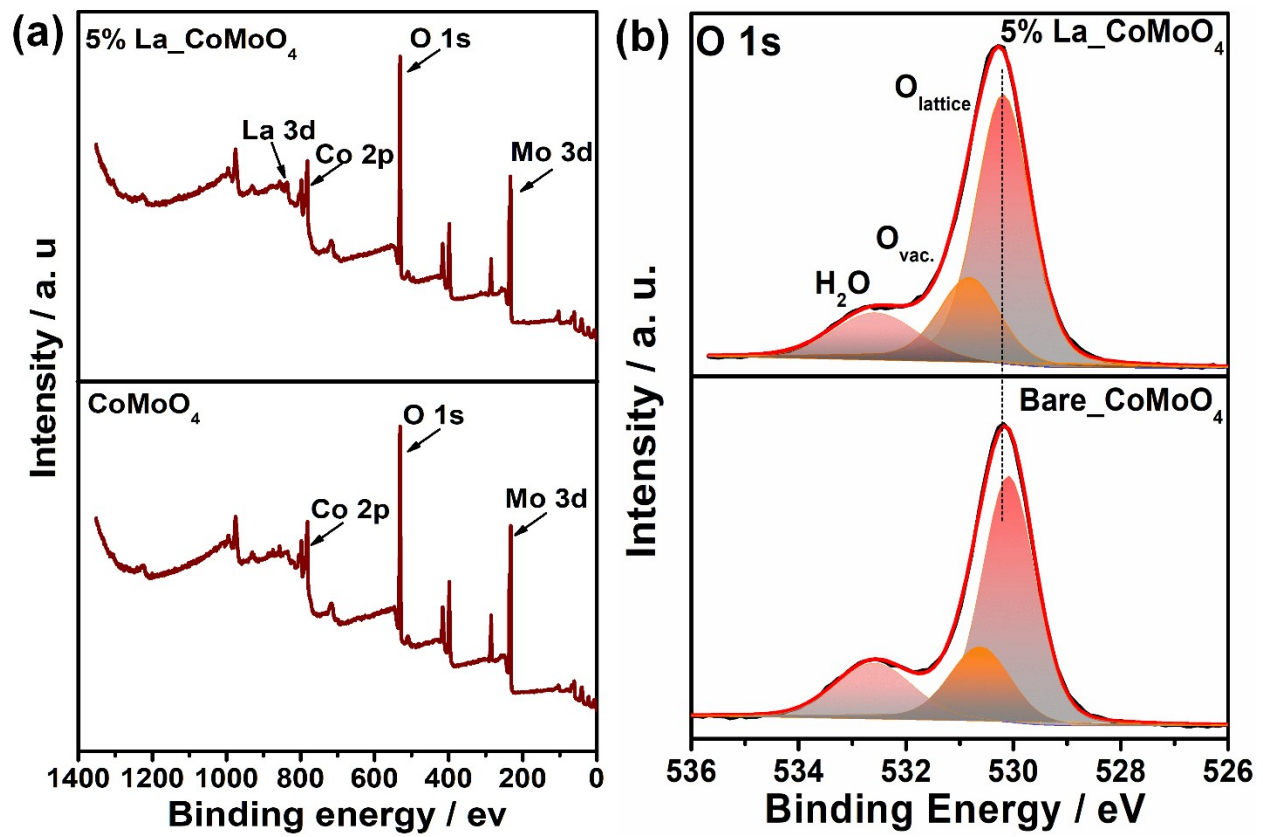


**Figure S7.** XPS wide-scan of (a) CoMoO<sub>4</sub> and 5% La<sub>x</sub>CoMoO<sub>4</sub>, (b) deconvoluted high-resolution spectra of CoMoO<sub>4</sub> and 5% La<sub>x</sub>CoMoO<sub>4</sub>.

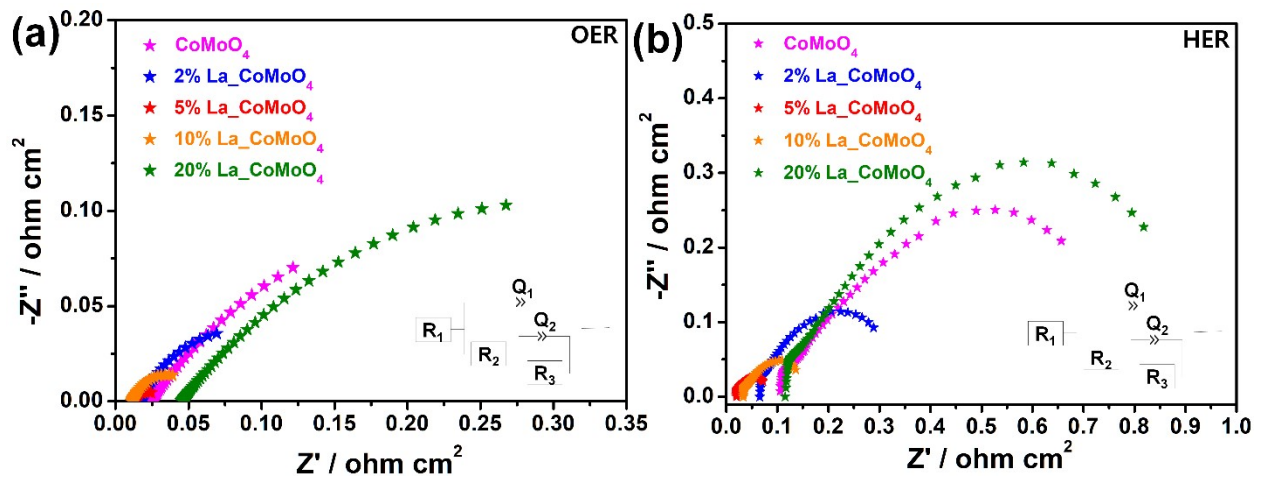


**Figure S8.** ECSA normalized Nyquist plots derived from electrochemical impedance spectra (EIS) of bare CoMoO<sub>4</sub>, 2% La\_CoMoO<sub>4</sub>, 5% La\_CoMoO<sub>4</sub>, 10% La\_CoMoO<sub>4</sub>, 20% La\_CoMoO<sub>4</sub> under anodic (1.5 V<sub>RHE</sub>) and cathodic (0.2 V<sub>RHE</sub>) bias. Insets are the corresponding equivalent circuit models used for fitting EIS spectra.

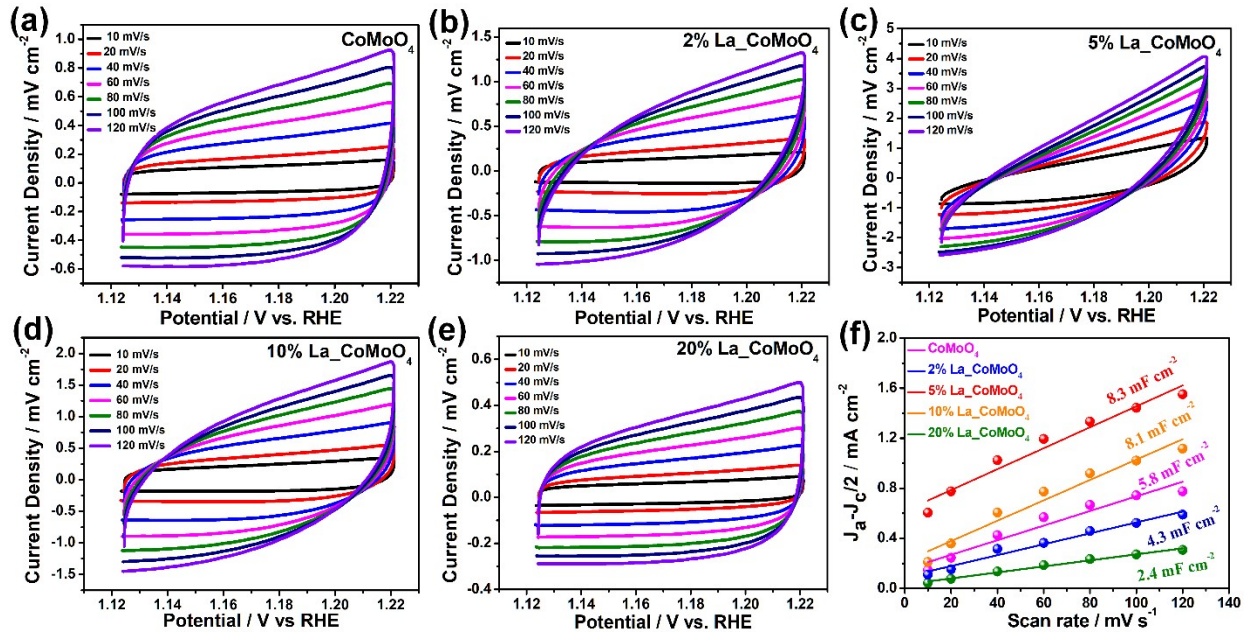


**Figure S9.** Non-faradaic CVs in anodic region of a) bare  $\text{CoMoO}_4$ , b) 2%  $\text{La}_{\text{CoMoO}}_4$ , c) 5%  $\text{La}_{\text{CoMoO}}_4$  d) 10%  $\text{La}_{\text{CoMoO}}_4$  e) 20%  $\text{La}_{\text{CoMoO}}_4$  f) corresponding  $C_{dl}$  estimation from  $\Delta J$  vs. scan rate plot.

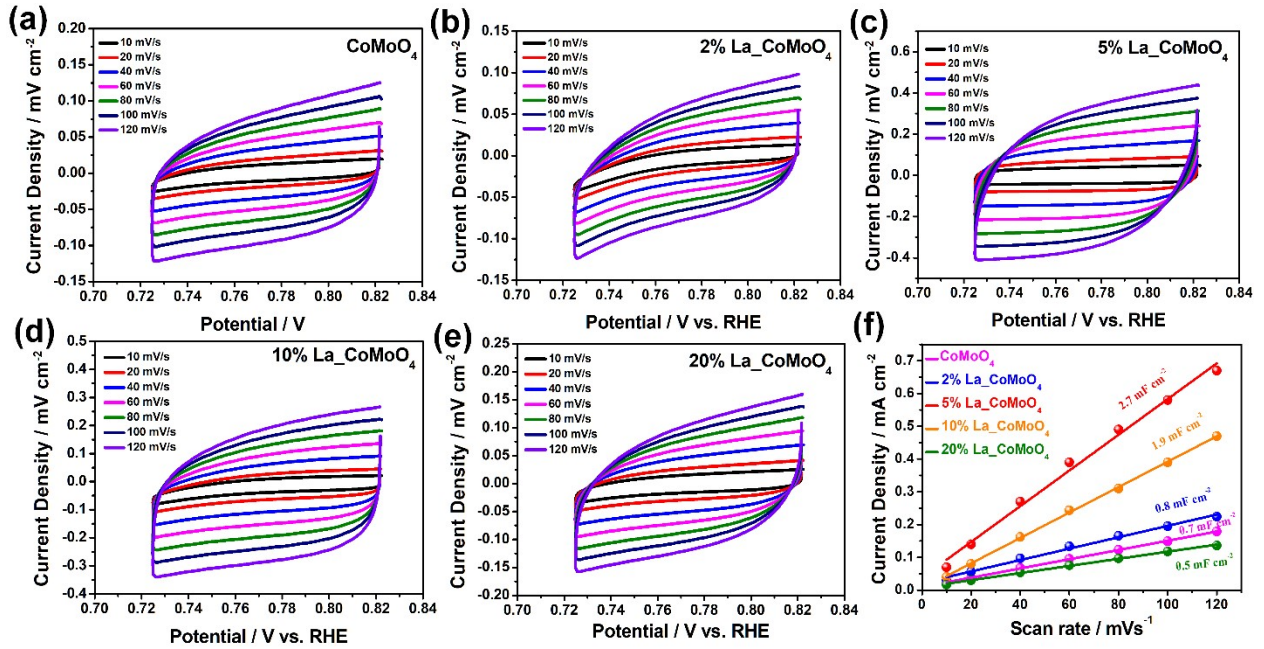


**Figure S10.** Non-faradaic CVs in cathodic region of a) bare  $\text{CoMoO}_4$ , b) 2%  $\text{La}_\text{CoMoO}_4$ , c) 5%  $\text{La}_\text{CoMoO}_4$ , d) 10%  $\text{La}_\text{CoMoO}_4$ , e) 20%  $\text{La}_\text{CoMoO}_4$ , f) corresponding  $C_{\text{dl}}$  estimation from  $\Delta J$  vs. scan rate plot.

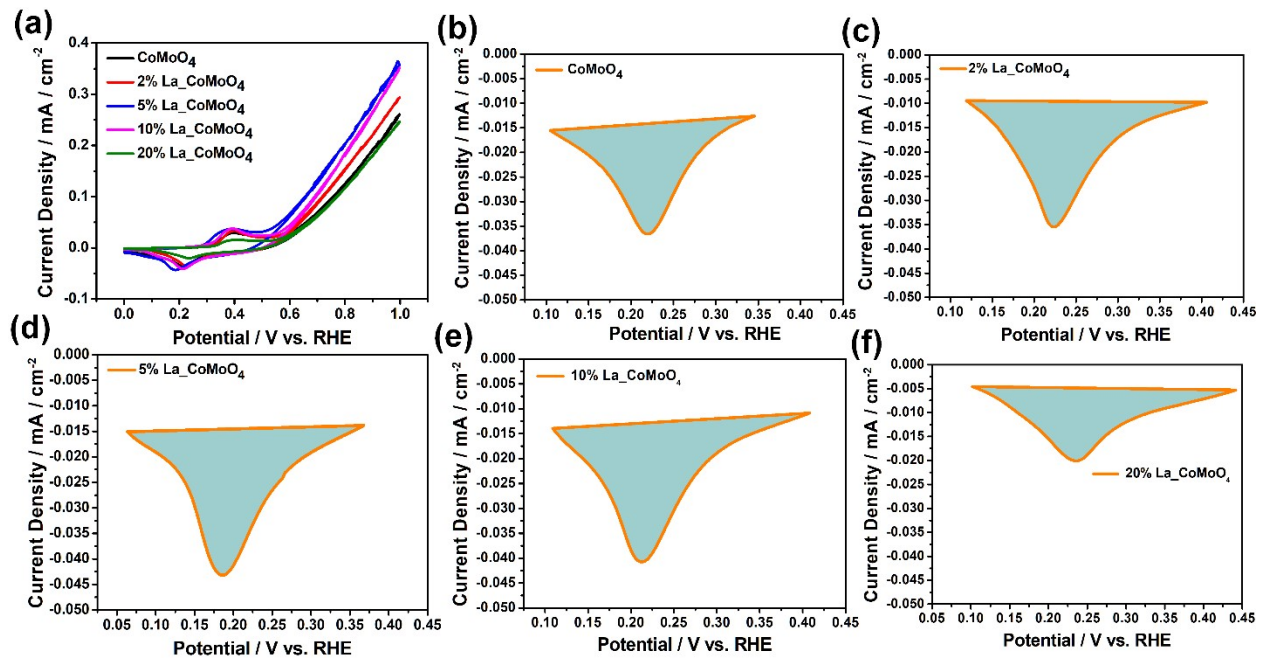


**Figure S11.** a) CVs comparision of bare CoMoO<sub>4</sub>, 2% La<sub>x</sub>CoMoO<sub>4</sub>, 5% La<sub>x</sub>CoMoO<sub>4</sub>, 10% La<sub>x</sub>CoMoO<sub>4</sub>, 20% La<sub>x</sub>CoMoO<sub>4</sub> depicting the redox peaks; integrated area of the reduction peaks for (a) bare CoMoO<sub>4</sub>, (b) 2% La<sub>x</sub>CoMoO<sub>4</sub>, (c) 5% La<sub>x</sub>CoMoO<sub>4</sub>, (d) 10% La<sub>x</sub>CoMoO<sub>4</sub>, (e) 20% La<sub>x</sub>CoMoO<sub>4</sub>.

### Turn Over Frequency Calculation (TOF)

The Turn Over Frequency was Calculated according to the reported equation 1

$$TOF = \frac{\text{total oxygen turnover} / \text{total hydrogen turnover} \times j}{\tau_0 \times ECSA} \quad (I)$$

$\tau_0$  = surface coverage of metal coated on the GC electrode

ECSA = electrochemical surface area The ECSA is calculated according to the reported literature using equation 2.

$$ECSA = \frac{Cdl}{cs} \quad (2)$$

$C_{dl}$  = double layer capacitance

$C_s$  = specific capacitance

Oxygen turnover calculated using Equation 3

$$Oxygen = \frac{j \times Na}{F \times 4 \times n} \quad (3)$$

Hydrogen turnover calculated using Equation 4

$$Hydrogen = \frac{j \times Na}{F \times 2 \times n} \quad (4)$$

j = current density at a fixed voltage (1.7V)

$N_a$  = Avogadro number ( $6.022 \times 10^{23}$  mol)

F = faraday constant (96485.329 C mol<sup>-1</sup>)

n = number of active sites

The calculation of the active sites is determined using equation 5 as described.

$$n = \frac{\text{charge (coulombs)}}{\text{charge of electron (coulombs)}} \quad (5)$$

The calculation of charge transfer can be determined by finding the area of redox peaks with Equation 6

$$\text{charge} = \frac{\text{Area of anodic or cathodic peak (AV)}}{\text{scan rate of CV (V/s)}} \quad (6)$$

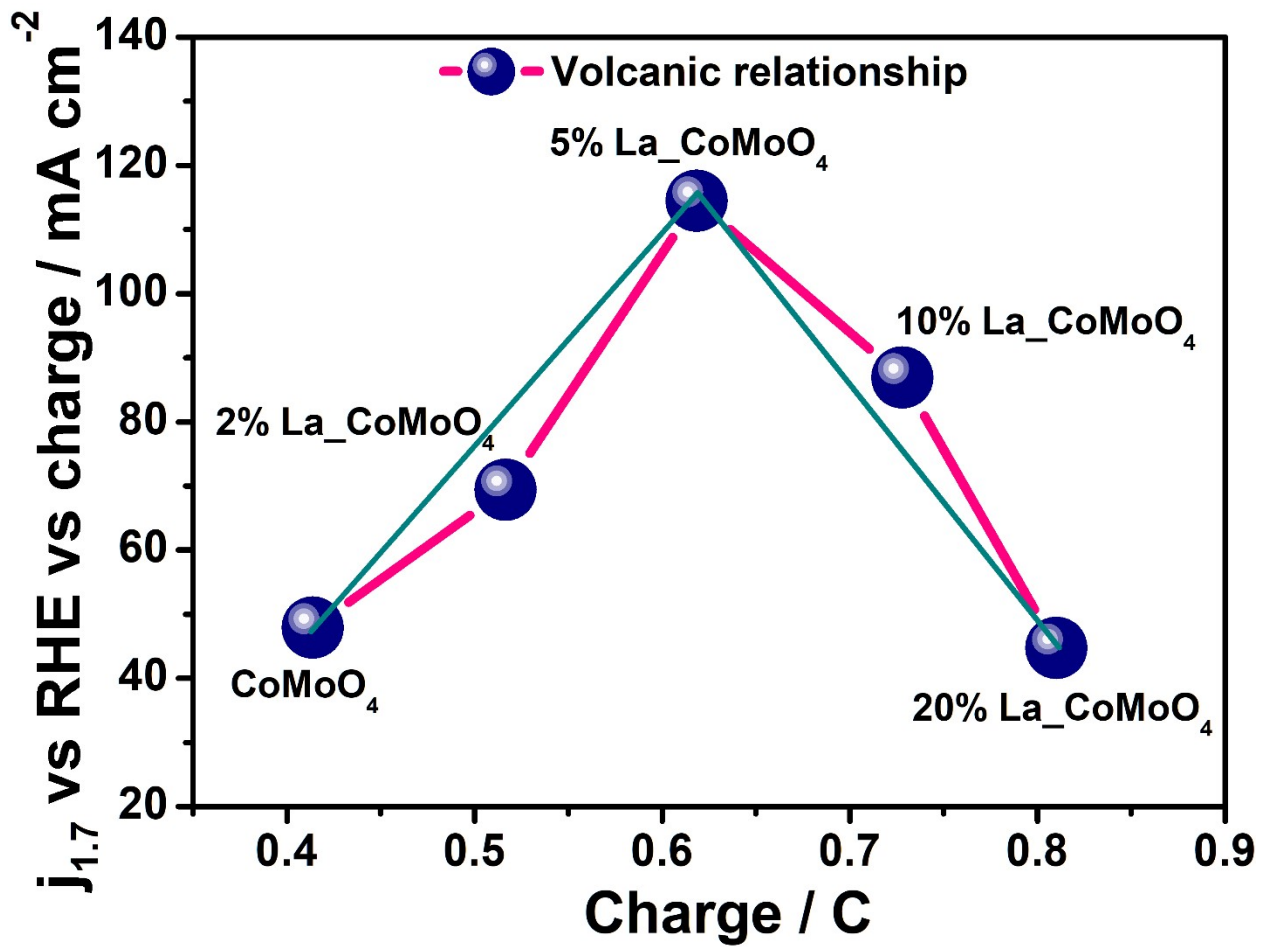


**Figure S12.**  $J_{1.7}$  V<sub>RHE</sub> vs. Charge / C plot of different percentages of La-doped CoMoO<sub>4</sub> electrocatalysts demonstrating volcanic relation.

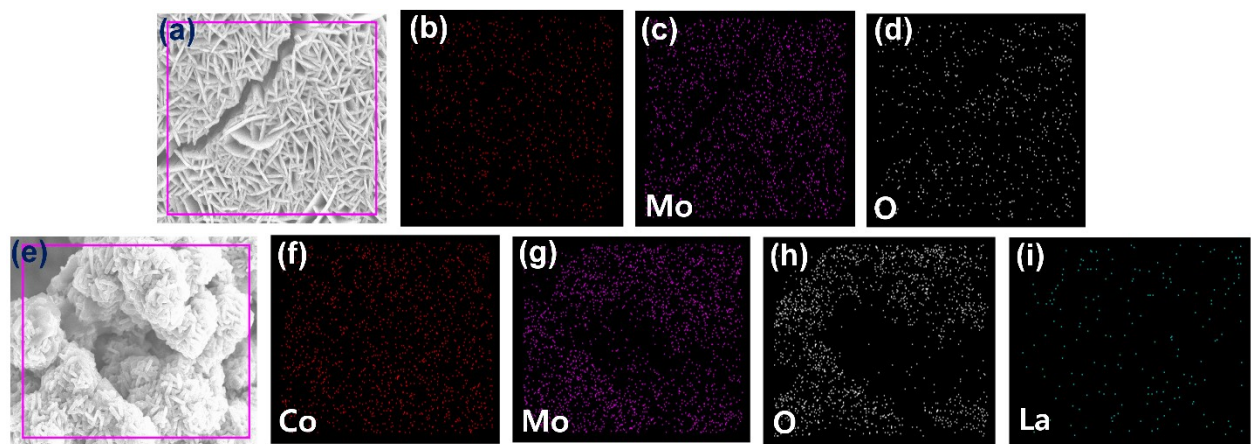


**Figure S13.** FESEM images and the corresponding energy dispersive X-ray (EDS) mapping analysis after 72 h stability study of (a-d) bare  $\text{CoMoO}_4$ , (e-i) 5%  $\text{La}_\text{-}\text{CoMoO}_4$ .

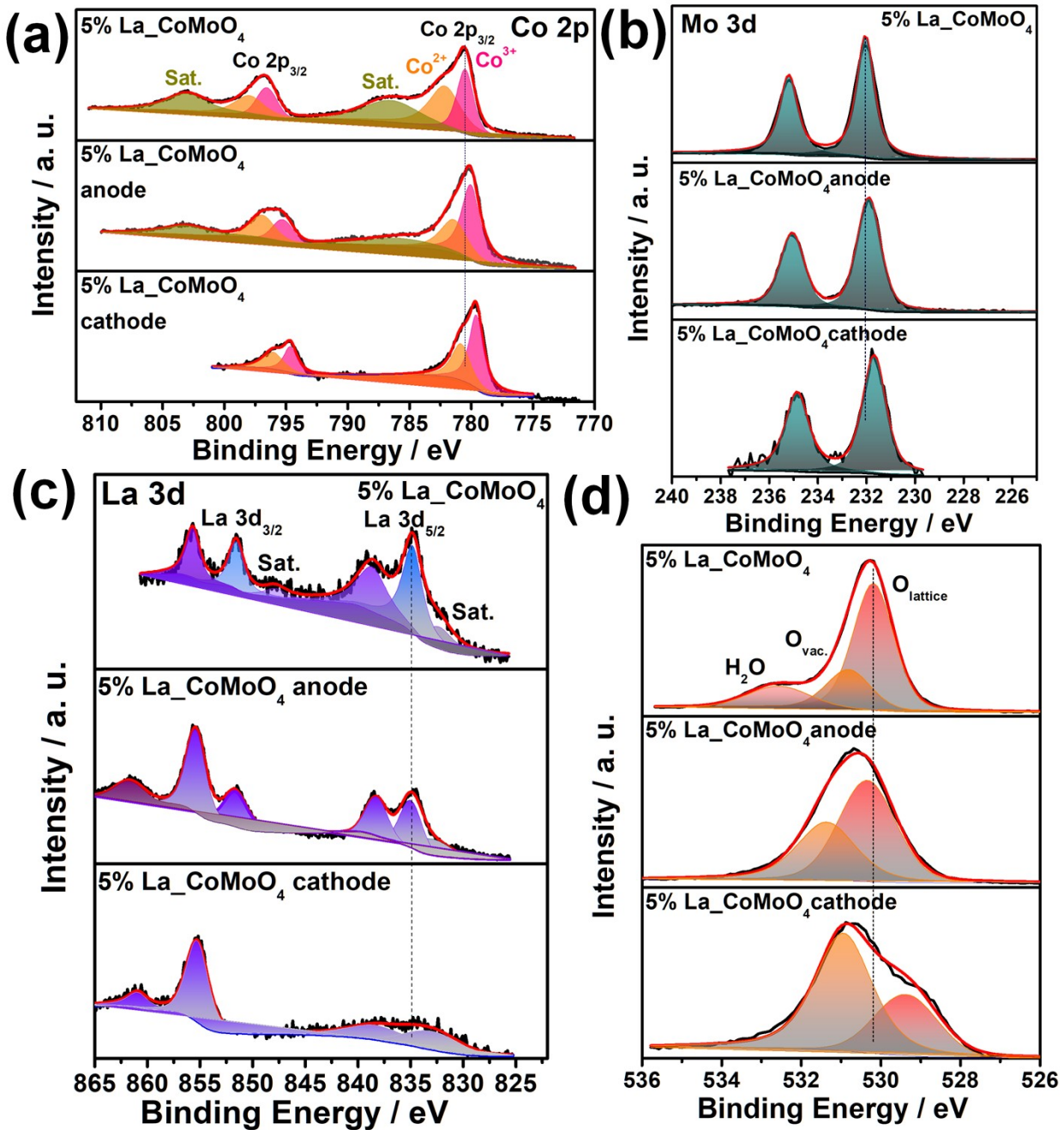


**Figure S14.** Post-catalysis XPS characterization. High-resolution XPS spectra of (a) Co 2p region for bare CoMoO<sub>4</sub>, 5% La<sub>x</sub>CoMoO<sub>4</sub> anode and 5% La<sub>x</sub>CoMoO<sub>4</sub> cathode electrode, (b) Mo 3d spectra of bare CoMoO<sub>4</sub>, 5% La<sub>x</sub>CoMoO<sub>4</sub> anode and 5% La<sub>x</sub>CoMoO<sub>4</sub> cathode electrodes, (c) La

3d region for bare CoMoO<sub>4</sub>, 5% La<sub>x</sub>CoMoO<sub>4</sub> anode and 5% La<sub>x</sub>CoMoO<sub>4</sub> cathode electrodes, (d)

O 1s spectra of bare CoMoO<sub>4</sub>, 5% La<sub>x</sub>CoMoO<sub>4</sub> anode and 5% La<sub>x</sub>CoMoO<sub>4</sub> cathode electrode.

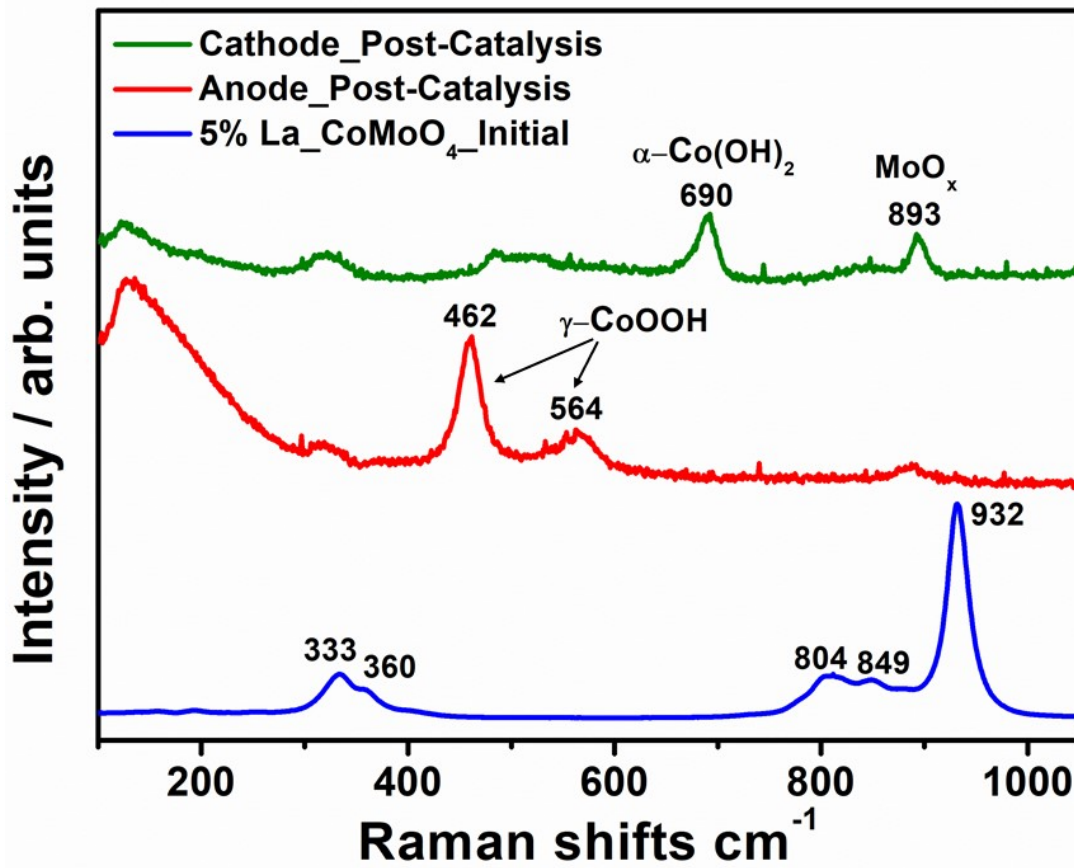


**Figure S15.** Post-catalysis Raman analyses of 5% La<sub>x</sub>CoMoO<sub>4</sub> post-catalyst before and after stability compared with initial as prepared 5% La<sub>x</sub>CoMoO<sub>4</sub> (anode and cathode) of the two-electrode system.

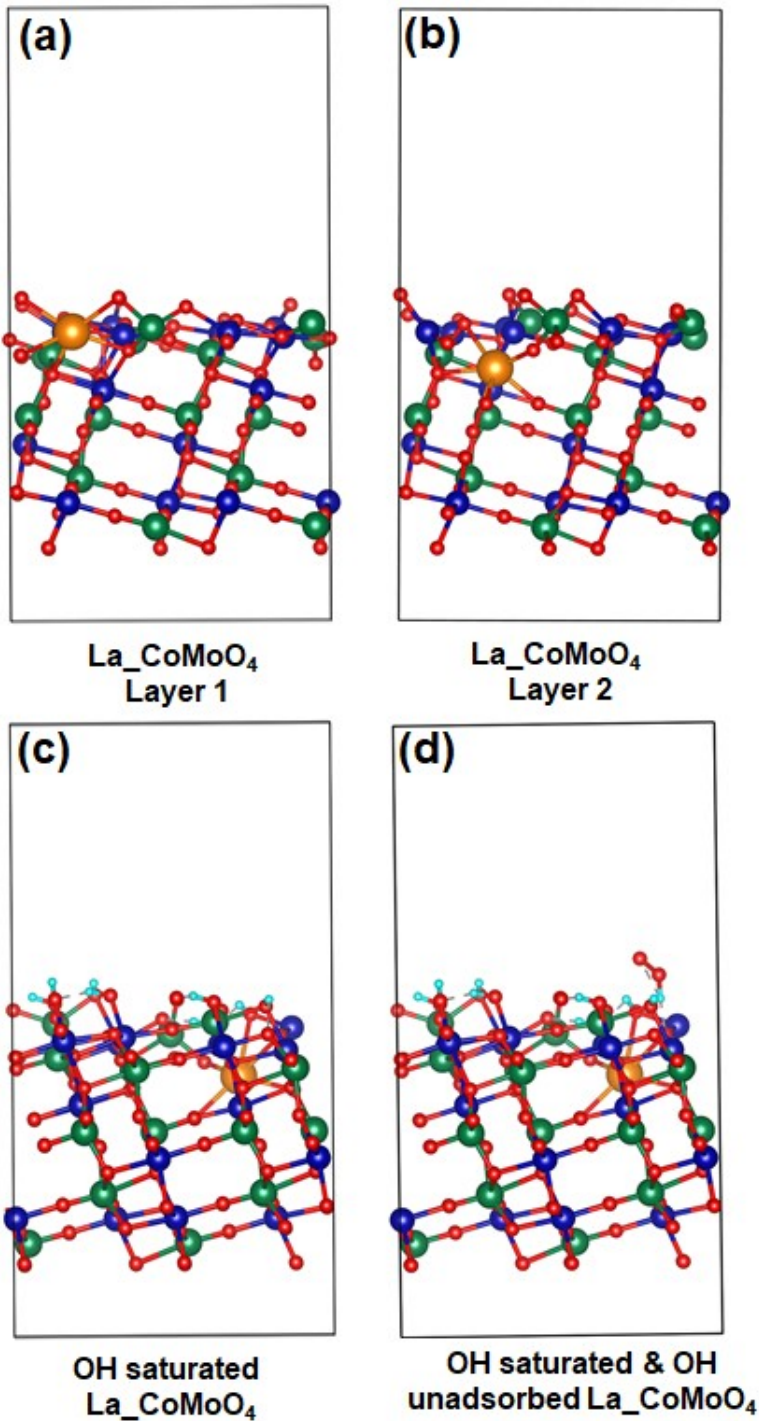


**Figure S16.** Unit cell models of La-doped CoMoO<sub>4</sub> in different configurations (a)  $\text{La}_\text{CoMoO}_4$  layer 1, (b)  $\text{La}_\text{CoMoO}_4$  layer 2, (c) OH adsorbed  $\text{La}_\text{CoMoO}_4$ , (d) OH adsorbed and unadsorbed  $\text{La}_\text{CoMoO}_4$ .

**Table S1.** Figure of merit for OER of different catalysts, bare CoMoO<sub>4</sub>, 2% La<sub>x</sub>CoMoO<sub>4</sub>, 5% La<sub>x</sub>CoMoO<sub>4</sub>, 10% La<sub>x</sub>CoMoO<sub>4</sub>, 20% La<sub>x</sub>CoMoO<sub>4</sub>.

S.No	Catalysts	Overpotential @ 20 mA cm <sup>-2</sup> (V)	Tafel (mV dec <sup>-1</sup> )	TOF (s <sup>-1</sup> )	C <sub>dl</sub> (mFcm <sup>-2</sup> )	ECSA (cm <sup>2</sup> )	R <sub>ct</sub> (ohm)
1	CoMoO <sub>4</sub>	0.390	63	0.0289	5.8	54.5	6.61
2	2% La <sub>x</sub> CoMoO <sub>4</sub>	0.370	53	0.0316	4.3	73	5.06
3	5% La <sub>x</sub> CoMoO <sub>4</sub>	0.272	41	0.0462	8.3	104.6	2.62
4	10% La <sub>x</sub> CoMoO <sub>4</sub>	0.347	50	0.0375	8.1	101.7	3.95
5	20% La <sub>x</sub> CoMoO <sub>4</sub>	0.390	67	0.2722	2.4	30.1	8.05

**Table S2.** Figure of merit for OER of different catalysts, bare CoMoO<sub>4</sub>, 2% La<sub>x</sub>CoMoO<sub>4</sub>, 5% La<sub>x</sub>CoMoO<sub>4</sub>, 10% La<sub>x</sub>CoMoO<sub>4</sub>, 20% La<sub>x</sub>CoMoO<sub>4</sub>.

S.No	Catalysts	Overpotential @ 20 mA cm <sup>-2</sup> (V)	Tafel (mV dec <sup>-1</sup> )	C <sub>dl</sub> (mFcm <sup>-2</sup> )	ECSA (cm <sup>2</sup> )	R <sub>ct</sub> (ohm)
1	CoMoO <sub>4</sub>	0.35	177	0.7	17.5	11.48
2	2% La <sub>x</sub> CoMoO <sub>4</sub>	0.318	72.5	0.8	21.2	6.12
3	5% La <sub>x</sub> CoMoO <sub>4</sub>	0.219	37.4	2.7	67.5	4.84
4	10% La <sub>x</sub> CoMoO <sub>4</sub>	0.272	52.6	1.9	47.5	6.47
5	20% La <sub>x</sub> CoMoO <sub>4</sub>	0.375	184	0.5	12.5	10.21

**Table S3.** EIS fitting parameters of bare CoMoO<sub>4</sub>, 2% La<sub>x</sub>CoMoO<sub>4</sub>, 5% La<sub>x</sub>CoMoO<sub>4</sub>, 10% La<sub>x</sub>CoMoO<sub>4</sub>, 20% La<sub>x</sub>CoMoO<sub>4</sub> for OER.

S. No	Catalysts	R <sub>s</sub> (ohm)	R <sub>ct</sub> (ohm)
1	CoMoO <sub>4</sub>	1.313	23.73
2	2% La <sub>x</sub> CoMoO <sub>4</sub>	1.225	9.811
3	5% La <sub>x</sub> CoMoO <sub>4</sub>	1.173	0.1032
4	10% La <sub>x</sub> CoMoO <sub>4</sub>	1.115	2.105
5	20% La <sub>x</sub> CoMoO <sub>4</sub>	1.35	15.45

**Table S4.** EIS fitting parameters of bare CoMoO<sub>4</sub>, 2% La<sub>x</sub>CoMoO<sub>4</sub>, 5% La<sub>x</sub>CoMoO<sub>4</sub>, 10% La<sub>x</sub>CoMoO<sub>4</sub>, 20% La<sub>x</sub>CoMoO<sub>4</sub> for OER for HER.

S. No	Catalysts	R <sub>s</sub> (ohm)	R <sub>ct</sub> (ohm)
1	CoMoO <sub>4</sub>	1.408	0.72
2	2% La <sub>x</sub> CoMoO <sub>4</sub>	1.929	0.5648
3	5% La <sub>x</sub> CoMoO <sub>4</sub>	1.643	0.355
4	10% La <sub>x</sub> CoMoO <sub>4</sub>	1.439	0.4211
5	20% La <sub>x</sub> CoMoO <sub>4</sub>	1.526	0.748

**Table S5.** ICP-OES analysis of different catalysts and after stability

Samples	Aliquot 1 (%)			Aliquot 2 (%)			Average (%)		
	Co	Mo	La	Co	Mo	La	Co	Mo	La
CoMoO <sub>4</sub>	31.45	46.64	0	31.84	48.54	0	31.64	47.59	0
2% La-CoMoO <sub>4</sub>	29.61	46.45	1.84	29.69	46.37	1.90	29.65	46.41	1.87
5% La-CoMoO <sub>4</sub>	27.26	45.83	4.79	27.02	46.11	4.74	27.14	45.97	4.76
10% La-CoMoO <sub>4</sub>	24.65	44.99	9.6	24.98	45.89	9.4	24.81	45.44	9.5
20% La-CoMoO <sub>4</sub>	22.84	45.46	19.85	22.64	45.98	19.56	22.74	45.72	19.7
5% La-CoMoO <sub>4</sub> After 72h stability	26.45	20.56	4.5	26.94	20.39	4.58	26.69	20.47	4.54
Leached MoO <sub>4</sub> in 1M KOH after 72h stability	0.41	25.22	0.21	0.43	25.26	0.18	0.42	25.24	0.19

**Table S6.** Comparison of the electrocatalytic OER performance of various competitive electrocatalysts and related rare-earth doped catalysts reported in the literature.

S. No	Catalyst	Overpotential (mV) @ 50 mA	Tafel slope (mV dec <sup>-1</sup> )	Electrolyte	Ref.
1.	5% La_CoMoO <sub>4</sub>	368	41	1M KOH	This work
2.	25% La-CoFe LDH	510	125	1M KOH	(6)
3.	5.6% Ce_LaCoO <sub>3</sub>	570	112	1M KOH	(7)
4.	CoMnNiFeZn/Fe <sub>2</sub> O <sub>4</sub>	440	53.6	1M KOH	(8)
5.	NiFeLa-8 LDH	380	73	1M KOH	(9)
6.	CoMo-MI-600	400	89.9	1M KOH	(10)
7.	Co <sub>3</sub> O <sub>4</sub> /La <sub>0.3</sub> Sr <sub>0.7</sub> CoO <sub>3</sub>	550	75	0.1M KOH	(11)
8.	1% La: $\alpha$ -Ni (OH) <sub>2</sub>	590	169.8	1M KOH	(12)
9.	Co-Mo-0.005-6N	370	106	1M KOH	(13)
10	LaSrCoO <sub>4</sub>	520	79.1	1M KOH	(14)
11	PrSrCoO <sub>4</sub>	500	83.4	1M KOH	(14)
12	Ce-Co (PO <sub>3</sub> ) <sub>2</sub> @NF	380	194	1M KOH	(15)
13	FeCo/Co <sub>2</sub> P	420	61	1M KOH	(16)
14	Mo-CoP (1/2.3)	420	82	1M KOH	(17)
15.	La-NiFe LDH-3	400	97.1	1M KOH	(18)

**Table S7.** Comparison of the electrocatalytic HER performance of various competitive electrocatalysts and related rare-earth doped catalysts reported in the literature.

S. No	Catalyst	Overpotential (mV) at 50mA cm <sup>-2</sup>	Tafel slope (mV dec <sup>-1</sup> )	Electrolyte	Ref.
1.	5% La <sub>x</sub> CoMoO <sub>4</sub>	309	37.4	1M KOH	This work
2.	LaSrCoO <sub>4</sub>	580	147.3	1M KOH	(14)
3.	PrSrCoO <sub>4</sub>	480	127.1	1M KOH	(14)
4.	SmSrCoO <sub>4</sub>	546	153.6	1M KOH	(14)
5.	EuSrCoO <sub>4</sub>	552	148.6	1M KOH	(14)
6.	GdSrCoO <sub>4</sub>	509	149.7	1M KOH	(14)
7.	Sr <sub>0.95</sub> Nb <sub>0.1</sub> Co <sub>0.9</sub> Ni <sub>x</sub> O <sub>3</sub>	370 @ 100 mV	80	1M KOH	(19)
8.	Sm@NiCu-LDH	347	109	1M KOH	(20)
9.	NiFePd LDH	400	135.8	1M KOH	(21)
10	β-Ni(OH) <sub>2</sub> nanoplatelets	480 @ 30mA	230	1M KOH	(22)
11	P-NiSe/NGr	500 @ 30mA	125	1M KOH	(23)
12	CoFe-LDH@g-C <sub>3</sub> N <sub>4</sub>	480	71	1M KOH	(24)
13	S-NiCo LDH/SS	410@20mV	69	1M KOH	(25)
14	MoO <sub>2</sub> /C	390	58.5	0.5M H <sub>2</sub> SO <sub>4</sub>	(26)
15	CoFe-LDH	590	95	1M KOH	(24)

**Table S8.** Comparison of the overall water splitting potential between our catalyst and the previously reported catalysts at 10 mA cm<sup>-2</sup>.

S. No	Catalyst	Potential (V) @ 10 mA cm <sup>-2</sup>	Ref
1.	5% La <sub>x</sub> CoMoO <sub>4</sub>	1.68	This work
2.	Co <sub>6</sub> Mo <sub>6</sub> C <sub>2</sub> /Co <sub>2</sub> Mo <sub>3</sub> O <sub>8</sub>	1.81	(2)
3.	CoMoS <sub>x</sub> /NF	1.74	(1)
4.	La-NiFe LDH	1.724	(3)
5.	Mo-CoP	1.7	(4)
6.	NiFePd LDH	1.74	(5)
7.	CoP/Graphene	1.725	(6)
8.	Co <sub>5.0</sub> MoP	1.769	(7)
9.	NiCoFeB	1.75	(8)
10.	FeS <sub>2</sub> @CoS <sub>2</sub>	1.8 @ 20 mA	(9)
11.	CoP@FeCoP/NC YSMPs	1.68	(10)
12.	Zn,S-CoP/CP	1.70	(11)
13.	CoP/GO-400	1.7	(12)
14.	(CoxP) NPs/ NC	1.71	(13)
15.	Mo <sub>2</sub> C/CS	1.73	(14)
16.	v-CoFe LDH	1.76	(15)
17.	Ni <sub>0.1</sub> Co <sub>0.9</sub> P/CP	1.89	(16)
18.	CoO/Co <sub>4</sub> N	1.79	(17)
19.	Fe-CoP/CC	1.95	(18)
20.	CoMnNiS-NF-31	1.80	(19)

## Reference

- (1) Kresse, G.; Furthmüller, J. Efficiency of Ab-Initio Total Energy Calculations for Metals and Semiconductors Using a Plane-Wave Basis Set. *Comput. Mater. Sci.* **1996**, *6* (1), 15–50.
- (2) Perdew, J. P.; Burke, K.; Ernzerhof, M. Generalized Gradient Approximation Made Simple. *Phys. Rev. Lett.* **1996**, *77* (18), 3865.
- (3) Blöchl, P. E. Projector Augmented-Wave Method. *Phys. Rev. B* **1994**, *50* (24), 17953.
- (4) Grimme, S.; Antony, J.; Ehrlich, S.; Krieg, H. A Consistent and Accurate Ab Initio Parametrization of Density Functional Dispersion Correction (DFT-D) for the 94 Elements H-Pu. *J. Chem. Phys.* **2010**, *132* (15), 154104. <https://doi.org/10.1063/1.3382344>.
- (5) Grimme, S.; Ehrlich, S.; Goerigk, L. Effect of the Damping Function in Dispersion Corrected Density Functional Theory. *J. Comput. Chem.* **2011**, *32* (7), 1456–1465. [https://doi.org/https://doi.org/10.1002/jcc.21759](https://doi.org/10.1002/jcc.21759).
- (6) Rong, M.; Zhong, H.; Wang, S.; Ma, X.; Cao, Z. La/Ce Doped CoFe Layered Double Hydroxides (LDH) Highly Enhanced Oxygen Evolution Performance of Water Splitting. *Colloids Surfaces A Physicochem. Eng. Asp.* **2021**, *625* (April). <https://doi.org/10.1016/j.colsurfa.2021.126896>.
- (7) Qian, J.; Wang, T.; Zhang, Z.; Liu, Y.; Li, J.; Gao, D. Engineered Spin State in Ce Doped LaCoO<sub>3</sub> with Enhanced Electrocatalytic Activity for Rechargeable Zn-Air Batteries. *Nano Energy* **2020**, *74* (May). <https://doi.org/10.1016/j.nanoen.2020.104948>.
- (8) No 主観的健康感を中心とした在宅高齢者における 健康関連指標に関する共分散構造分析 Title. *J. Sains dan Seni ITS* **2017**, *6* (1), 51–66.
- (9) Xu, R.; Wang, X.; Yang, Z.; Chang, Y.; Chen, X.; Wang, J.; Li, H. Electrodeposition Fabrication of La-Doped NiFe Layered Double Hydroxide to Improve Conductivity for Efficient Overall Water Splitting. *ACS Appl. Energy Mater.* **2024**. <https://doi.org/10.1021/acsadm.4c00246>.
- (10) Guo, Y.; Huang, Q.; Ding, J.; Zhong, L.; Li, T. T.; Pan, J.; Hu, Y.; Qian, J.; Huang, S. CoMo Carbide/Nitride from Bimetallic MOF Precursors for Enhanced OER Performance. *Int. J. Hydrogen Energy* **2021**, *46* (43), 22268–22276. <https://doi.org/10.1016/j.ijhydene.2021.04.084>.
- (11) Wang, X.; Pan, Z.; Chu, X.; Huang, K.; Cong, Y.; Cao, R.; Sarangi, R.; Li, L.; Li, G.; Feng, S. Atomic-Scale Insights into Surface Lattice Oxygen Activation at the Spinel/Perovskite Interface of Co<sub>3</sub>O<sub>4</sub>/La<sub>0.3</sub>Sr<sub>0.7</sub>CoO<sub>3</sub>. *Angew. Chemie - Int. Ed.* **2019**, *58* (34), 11720–11725. <https://doi.org/10.1002/anie.201905543>.
- (12) Wei, Z.; Sun, W.; Liu, S.; Qi, J.; Kang, L.; Li, J.; Lou, S.; Xie, J.; Tang, B.; Xie, Y. Particuology for Robust Bifunctional Electro-Oxidation. **2021**, *57*, 104–111.
- (13) Zhang, X.; Wu, A.; Wang, D.; Jiao, Y.; Yan, H.; Jin, C.; Xie, Y.; Tian, C. Fine-Tune the Electronic Structure in Co-Mo Based Catalysts to Give Easily Coupled HER and OER Catalysts for Effective Water Splitting. *Appl. Catal. B Environ.* **2023**, *328* (February). <https://doi.org/10.1016/j.apcatb.2023.122474>.
- (14) Huang, Y.; Hu, J.; Li, J.; Xie, W.; Xu, H. S.; Tang, K. Study on Water Splitting of the 214-Type Perovskite Oxides LnSrCoO<sub>4</sub> (Ln = La, Pr, Sm, Eu, and Ga). *Langmuir* **2024**, *40* (19), 9965–9974. <https://doi.org/10.1021/acs.langmuir.4c00079>.

- (15) Yang, Y.; Xiong, Y.; Zhou, Q.; Yang, J.; Qian, D.; Hu, Z. Ce Doped Co(PO<sub>3</sub>)<sub>2</sub>@NF Bifunctional Electrocatalyst for Water Decomposition. *Mater. Sci. Eng. B* **2023**, *290* (October 2022). <https://doi.org/10.1016/j.mseb.2023.116344>.
- (16) Nadarajan, R.; Gopinathan, A. V.; Dileep, N. P.; Sidharthan, A. S.; Shajumon, M. M. Heterointerface Engineering of Cobalt Molybdenum Suboxide for Overall Water Splitting. *Nanoscale* **2023**, *15* (37), 15219–15229. <https://doi.org/10.1039/d3nr02458j>.
- (17) Li, L.; Guo, Y.; Wang, X.; Liu, X.; Lu, Y. Ultraeven Mo-Doped CoP Nanocrystals as Bifunctional Electrocatalyst for Efficient Overall Water Splitting. *Langmuir* **2021**, *37* (19), 5986–5992. <https://doi.org/10.1021/acs.langmuir.1c00524>.
- (18) Yu, J.; Lu, K.; Wang, C.; Wang, Z.; Fan, C.; Bai, G.; Wang, G.; Yu, F. Modification of NiFe Layered Double Hydroxide by Lanthanum Doping for Boosting Water Splitting. *Electrochim. Acta* **2021**, *390*, 138824. <https://doi.org/10.1016/j.electacta.2021.138824>.
- (19) Islam, Q. A.; Majee, R.; Bhattacharyya, S. Bimetallic Nanoparticle Decorated Perovskite Oxide for State-of-the-Art. **2019**.
- (20) Singha Roy, S.; Karmakar, A.; Madhu, R.; Nagappan, S.; N Dhandapani, H.; Kundu, S. Three-Dimensional Sm-Doped NiCu-LDH on Ni Foam as a Highly Robust Bifunctional Electrocatalyst for Total Water Splitting. *ACS Appl. Energy Mater.* **2023**, *6* (17), 8818–8829. <https://doi.org/10.1021/acsaem.3c01338>.
- (21) Liu, D.; Liu, J.; Xue, B.; Zhang, J.; Xu, Z.; Wang, L.; Gao, X.; Luo, F.; Li, F. Bifunctional Water Splitting Performance of NiFe LDH Improved by Pd<sup>2+</sup> Doping. *ChemElectroChem* **2023**, *10* (4), 1–9. <https://doi.org/10.1002/celc.202201025>.
- (22) Balčiūnaitė, A.; Upadhyay, K. K.; Radinović, K.; Santos, D. M. F.; Montemor, M. F.; Šljukić, B. Steps towards Highly-Efficient Water Splitting and Oxygen Reduction Using Nanostructured β-Ni(OH)<sub>2</sub>. *RSC Adv.* **2022**, *12* (16), 10020–10028. <https://doi.org/10.1039/d2ra00914e>.
- (23) Nadeema, A.; Walko, P. S.; Devi, R. N.; Kurungot, S. Alkaline Water Electrolysis by NiZn-Double Hydroxide-Derived Porous Nickel Selenide-Nitrogen-Doped Graphene Composite. *ACS Appl. Energy Mater.* **2018**, *1* (10), 5500–5510. <https://doi.org/10.1021/acsaem.8b01081>.
- (24) Arif, M.; Yasin, G.; Shakeel, M.; Mushtaq, M. A.; Ye, W.; Fang, X.; Ji, S.; Yan, D. Hierarchical CoFe-Layered Double Hydroxide and g-C<sub>3</sub>N<sub>4</sub> Heterostructures with Enhanced Bifunctional Photo/Electrocatalytic Activity towards Overall Water Splitting. *Mater. Chem. Front.* **2019**, *3* (3), 520–531. <https://doi.org/10.1039/c8qm00677f>.
- (25) Karthik, N.; Edison, T. N. J. I.; Atchudan, R.; Xiong, D.; Lee, Y. R. Electro-Synthesis of Sulfur Doped Nickel Cobalt Layered Double Hydroxide for Electrocatalytic Hydrogen Evolution Reaction and Supercapacitor Applications. *J. Electroanal. Chem.* **2019**, *833* (November 2018), 105–112. <https://doi.org/10.1016/j.jelechem.2018.11.028>.
- (26) Guo, J.; Wang, J.; Wu, Z.; Lei, W.; Zhu, J.; Xia, K.; Wang, D. Controllable Synthesis of Molybdenum-Based Electrocatalysts for a Hydrogen Evolution Reaction. *J. Mater. Chem. A* **2017**, *5* (10), 4879–4885. <https://doi.org/10.1039/c6ta10758c>.